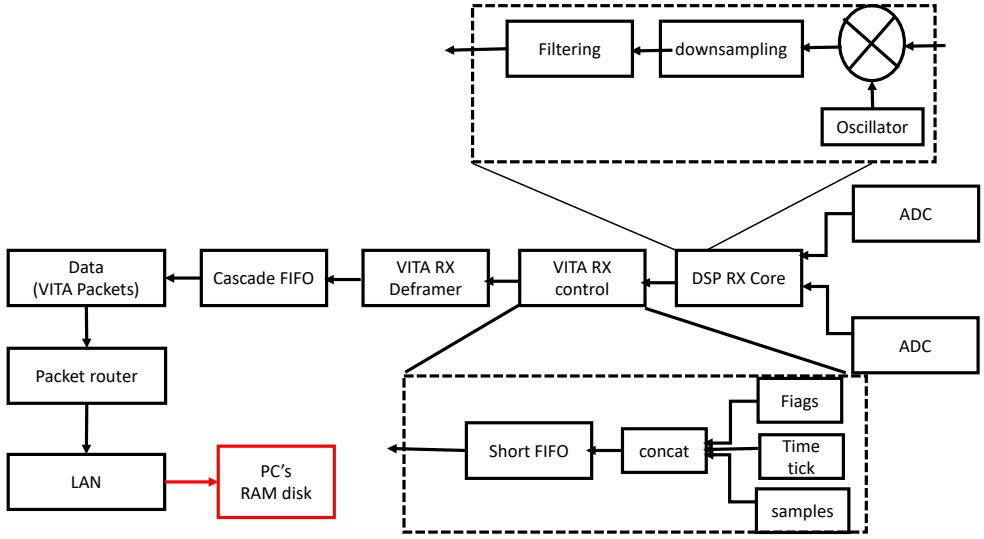

(b) Rx-side structure

Figure 1. The USRP DSP chain structure (a) Tx-side (b) Rx-side

In this system architecture, we found that the link between the DSP chain and the control PC becomes a bottleneck of the entire data processing due to inferior throughput performance of hard disk (HD) of the control PCs. Therefore we have proposed to utilize the RAM disk of the control PC[15]. As shown in Figure 1, the transmitted signal is stored into the RAM disk of the Tx-side host PC before the measurement. The received signal is also stored in the RAM disk of the Rx-side host PC during the measurement. The channel characteristics are evaluated from the stored data in the RAM by off-line data processing. By this improvement, wideband channel measurement signals can be recorded without sampling loss.

Directional Channel Measurement

Figure 2 shows the developed virtual antenna array method for measurements of directional channel properties. The Tx and Rx antennas are patch antennas and fixed on the rotators. The rotators are controlled by the rotation control PC, and the USRP Tx/Rx nodes are controlled by their control PCs which were connected each other by Ethernet. In the measurement, the Tx control PC firstly triggers both the USRP Tx node and the Rx control PC to start the measurement. After the Rx control PC finishes receiving the signal, it triggers the rotation control PC to start rotating. Finally, when the rotator finishes rotating, it triggers the Tx control PC to start the measurement again. The measurements continue automatically until all measurements of all antenna direction conditions finish.

We assume a static propagation environment in which the propagation channel remains unchanged during a whole measurement. Through the virtual array based measurement, the frequency channel transfer function matrix $\mathbf{H}[n] = (h_{k,l}[n])$ of each Rx/Tx azimuth angle condition is obtained. Here, $k\,(0 \le k \le K-1)$ is the Rx antenna rotation index, $l\,(0 \le l \le L-1)$ is the Tx antenna direction rotation and $n\,(0 \le n \le N-1)$ is the sub-carrier index, respectively. In this paper, we assume the same rotation step for both Tx and Rx sides, that means $K = L$. The channel impulse response matrix $\mathbf{G}[m] = (g_{k,l}[m])$ is calculated by inverse Fourier transform of the transfer function defined as follow.

$$g_{k,l}[m] = \frac{1}{N}\sum_{n=0}^{N-1} \zeta W[n] h_{k,l}[n] \exp(j\frac{2\pi nm}{N}) \quad (1)$$

Here, $m\,(0 \le m \le M-1)$ is the time sampling index, $W[n]$ is the Hanning window function to suppress a side lobe level, and $\zeta = N \Big/ \sum_{n=0}^{N-1} W[n]$. The angular power spectrum is calculated for the evaluation of the directional properties of the channel. Tx/Rx antenna array responses $\boldsymbol{\alpha}_{\mathrm{T}}(\phi_{\mathrm{T}}, n)$, $\boldsymbol{\alpha}_{\mathrm{R}}(\phi_{\mathrm{R}}, n)$ are calculated from the theoretical mode vector of the uniform circular array (UCA) and the patch antenna's radiation pattern $p(\phi, n)$. Here, ϕ_{T} and ϕ_{R} represent the azimuth angle-of-departure (AoDazm) and the azimuth angle-of-arrival (AoAazm), respectively.

$$\begin{aligned}\boldsymbol{\alpha}_{\mathrm{T/R}}(\phi_{\mathrm{T/R}}, n) = [\, & p(\phi_{\mathrm{T/R}}, n)\exp(j\frac{2\pi r\cos(\phi_{\mathrm{T/R}})}{\lambda_n}),\ p(\phi_{\mathrm{T/R}} - \Delta\eta, n)\exp(j\frac{2\pi r\cos(\phi_{\mathrm{T/R}} - \Delta\eta)}{\lambda_n}) \\ & \ldots p(\phi_{\mathrm{T/R}} - (L-1)\Delta\eta, n)\exp(j\frac{2\pi r\cos(\phi_{\mathrm{T/R}} - (L-1)\Delta\eta)}{\lambda_n})\,]\end{aligned} \quad (2)$$

Here, λ_n is the wavelength of the carrier wave, r is the antenna rotation radius, and $\Delta\eta = 2\pi/L$. Finally, the double directional angular power spectrum is defined as follows.

$$Y(\phi_{\mathrm{R}}, \phi_{\mathrm{T}}) = \sum_{n=0}^{N-1} \frac{|\, \boldsymbol{\alpha}_R^{\mathrm{H}}(\phi_{\mathrm{R}}, n)\mathbf{H}(n)\boldsymbol{\alpha}_T^{*}(\phi_{\mathrm{T}}, n)\,|^2}{|\, \boldsymbol{\alpha}_R(\phi_{\mathrm{R}}, n)\,|^2 |\, \boldsymbol{\alpha}_T(\phi_{\mathrm{T}}, n)\,|^2} \quad (3)$$

The Tx-side and the Rx-side angular power spectra $Y_{\mathrm{T}}(\phi_{\mathrm{T}}), Y_{\mathrm{R}}(\phi_{\mathrm{R}})$ are also defined from $Y(\phi_{\mathrm{R}}, \phi_{\mathrm{T}})$ as follows.

$$Y_{\mathrm{T}}(\phi_{\mathrm{T}}) = \int_0^{2\pi} Y(\phi, \phi_{\mathrm{T}})\, d\phi \quad (4)$$

$$Y_{\mathrm{R}}(\phi_{\mathrm{R}}) = \int_0^{2\pi} Y(\phi_{\mathrm{R}}, \phi)\, d\phi \quad (5)$$

Performance Evaluations of Developed Channel Sounder

Packet Loss Characteristics

To justify the performance improvement of the proposed method which utilizes the RAM of control PC, we evaluated the packet loss characteristics between the Rx control PC and the USRP Rx. In the test, the Tx and the Rx are directly connected by the RF cable. The Rx continuously recorded the data which were sent from the Tx for10 sec. Measurement parameters are shown in Table I (a). In the first test, the data were recorded to the HD of Rx PC, and in the next test, the data were recorded to the RAM of Rx PC. We repeated the tests for 10 times for each case.

Figure 3(a) shows the packet loss transition of a trial in the HD case. The packet losses occurred in bursts owing to the buffer overflow of the Rx PC. It is thought to be a reason for the sounding performance degradation. Figure 3(b) presents the average packet

loss ratios of all tests. In the HD case, the packet loss ratios ranged from 0.0030 to 0.0085 owing to this problem. However, it was suppressed less than 0.0002 by utilizing the RAM.

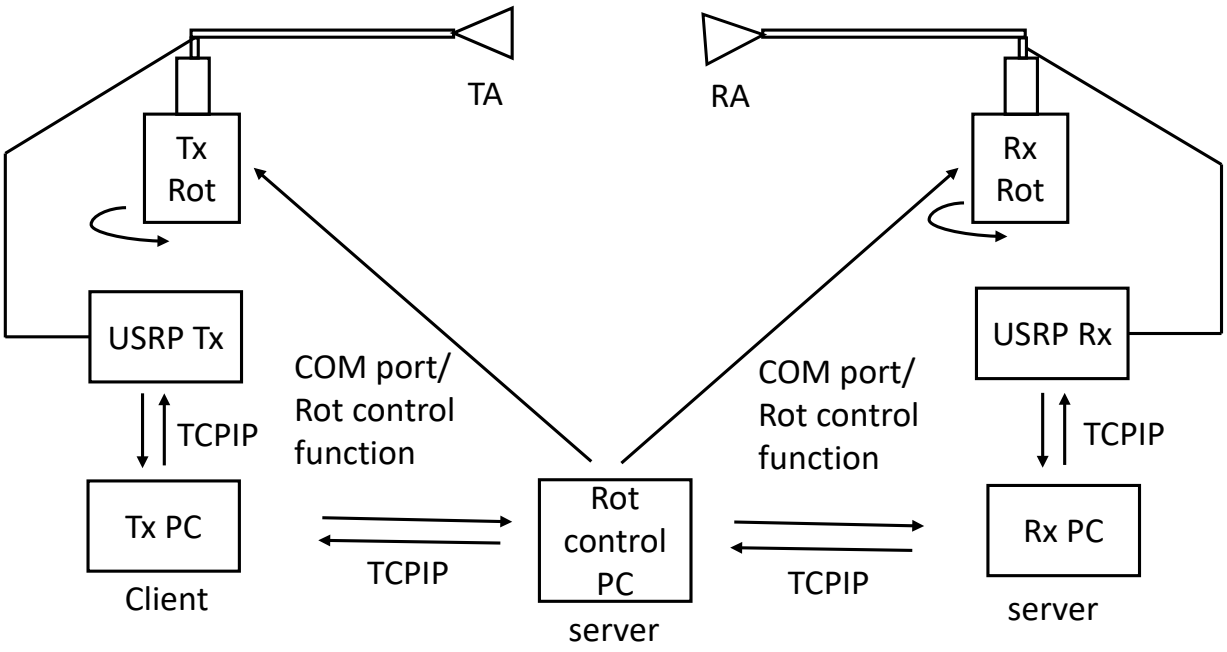

Figure 2. The channel sounder structure for directional channel measurement

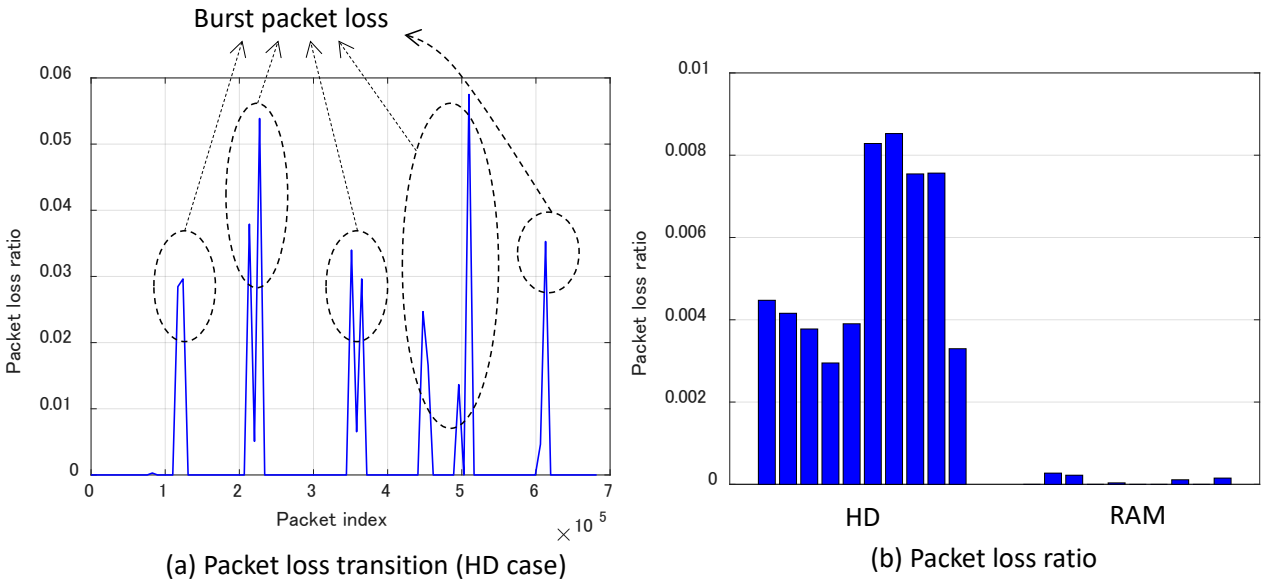

Figure 3 The packet loss characteristics (a) Packet loss transition example (HD case), (b) Packet loss ratio comparison

Baseband Signal Processing Performance

The baseband signal processing performance of the developed channel sounder was evaluated by a T-junction cable connected test. The test overview is shown in Figure 4.

The test system consisted of a cable which was directly connected to the Tx and the Rx, and a cable of which one side was kept open, and attenuators. The local oscillators of the Tx and the Rx were synchronized with the 10MHz reference of an external rubidium clock.

Firstly, the S12 parameter of the test system was measured by the VNA (Rohde & Schwartz ZVA 40) for the reference. Next, the developed channel sounder was connected to the test system, and then the channel transfer function was measured. Measurement parameters are shown in Table I.

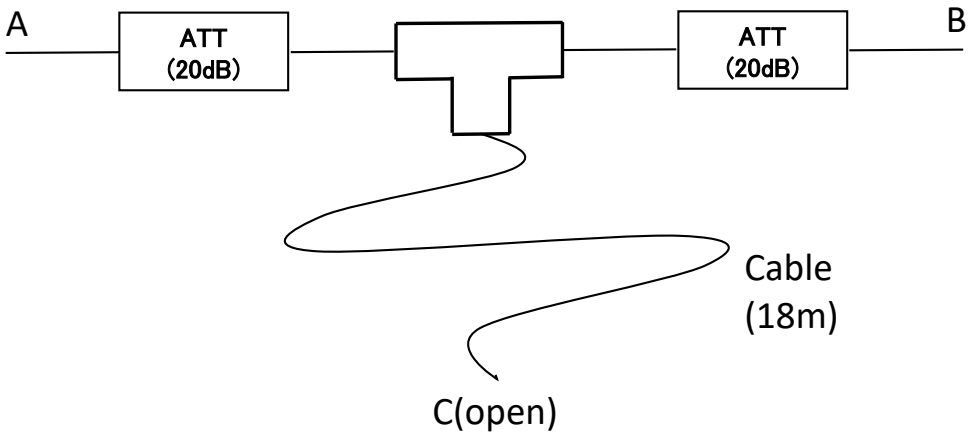

(a) T-junction cable connected test scheme

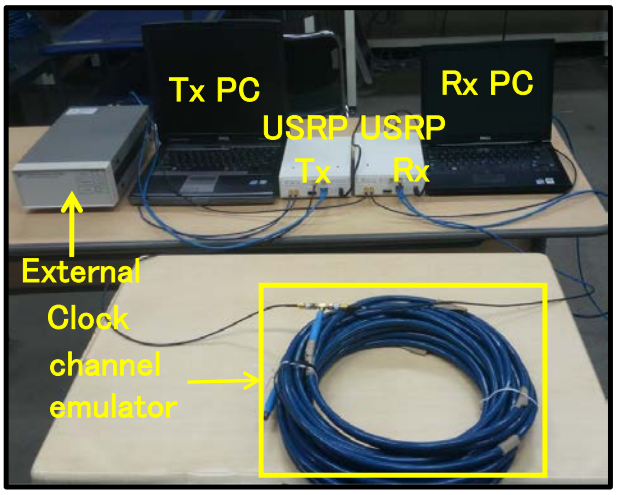

(b) The Test for the USRP-based system

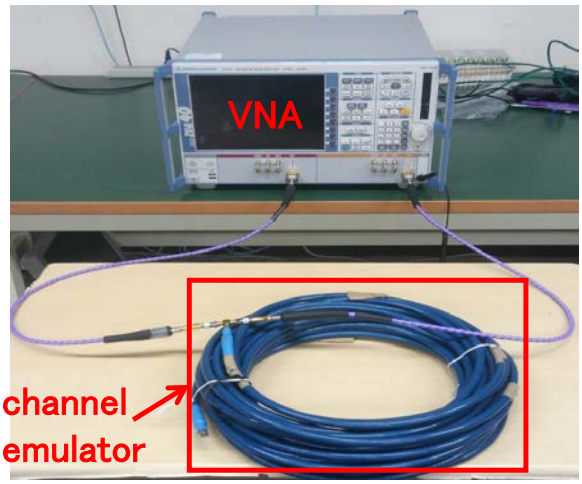

(c) The Test for the VNA-based system

Figure 4. The baseband signal processing performance evaluation (a) T-junction cable connected test scheme, (b) The Test for the USRP-based system, (c) The Test for the VNA-based system

Table I. Measurement parameters

Value	(a) USRP channel sounder	(b) VNA (R&S ZVA40)
Carrier frequency	2.4 GHz	2.4 GHz
Bandwidth	12.5 MHz	12.5 MHz
Frequency points	128	128
Transmit power	5 dBm	5 dBm
Transmit signal	Multitone	Frequency sweep
Sampling rate	25 MSps	-

The amplitudes of the measured channel impulse responses are shown in Figure 5(a). There were two peaks at 80 ns and 240 ns, respectively. It is thought that the first peak corresponded to the signal which propagated through the cable that is connected between the Tx and the Rx directly. The second peak corresponded to the signal which propagated to the Rx after the round trip through the cable of which one side was kept open. Those peaks were detected correctly by both the USRP channel sounder and the VNA. Figure 5 (b) shows the phases of the measured channel transfer functions. The phase difference of the USRP channel sounder and the VNA was 2 deg. at a maximum, and it is thought that the data were sampled at correct timings without any sampling losses.

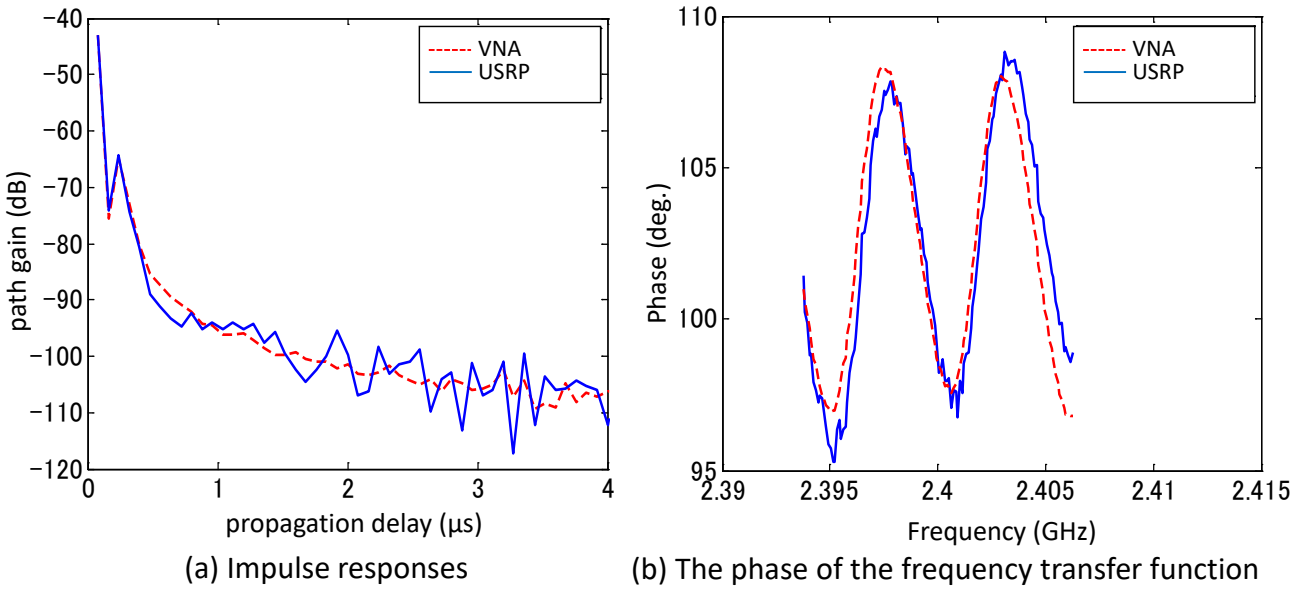

(a) Impulse responses (b) The phase of the frequency transfer function

Figure 5. The measurement result (a) Impulse responses, (b) The phase of the frequency transfer function

Angular Power Spectrum Comparison in an Indoor Environment

Channel measurements were conducted in a room environment, and the angular power spectra obtained by both the USRP-based system and the VNA-based system were

compared. The room layout is shown in Figure 6. The room size was approximately 6.7 m × 5.5 m. There were a lot of fixtures such as wooden desks, steel shelves, steel carts, and small objects like measurement equipment. The spectra were calculated by using the virtual antenna array method that is described in Section 2.2. The center frequency was 2.4 GHz. Patch antennas were mounted on tripods which were connected to rotators.

Both the Tx and the Rx antenna heights were 1.3 m. The number of virtual UCA elements was 36, and the rotation radius was 0.358 m so as to set the antenna spacing to the half wavelength of the carrier wave. In the measurement, both the Tx antenna and the Rx antennas were rotated to obtain the double directional angular power spectrum. The same measurements were conducted by using both the developed USRP-based system and the VNA-based system for comparisons. Other measurement parameters were same as Table I.

The AoA azimuth - AoD azimuth domain angular power spectrum measured by the USRP-based system and the VNA-based system are shown in Figure 7. In the results, three significant clusters were observed. It is thought that the propagation channel consisted of the LoS cluster which was marked by the yellow circle and single bounce clusters.

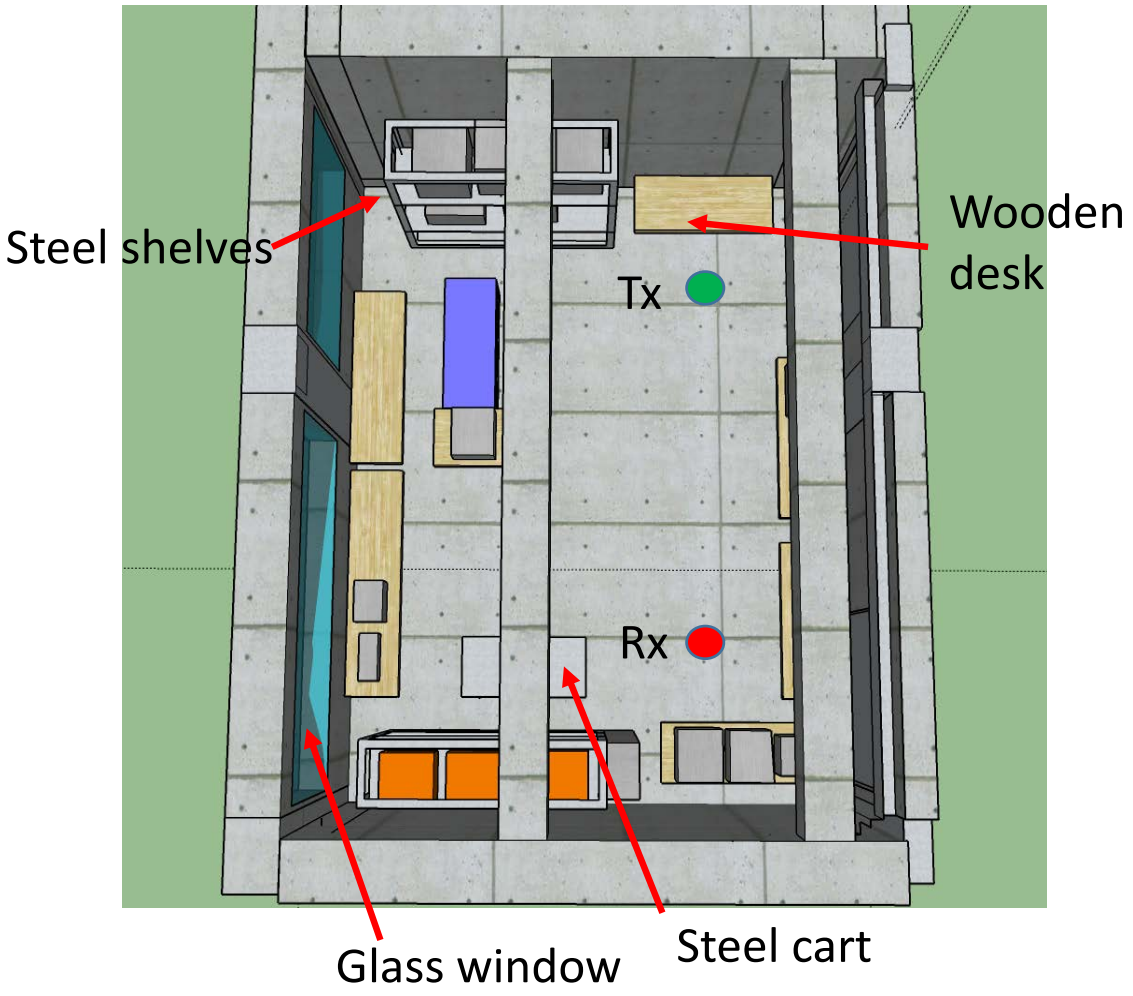

Figure 6. The room layout

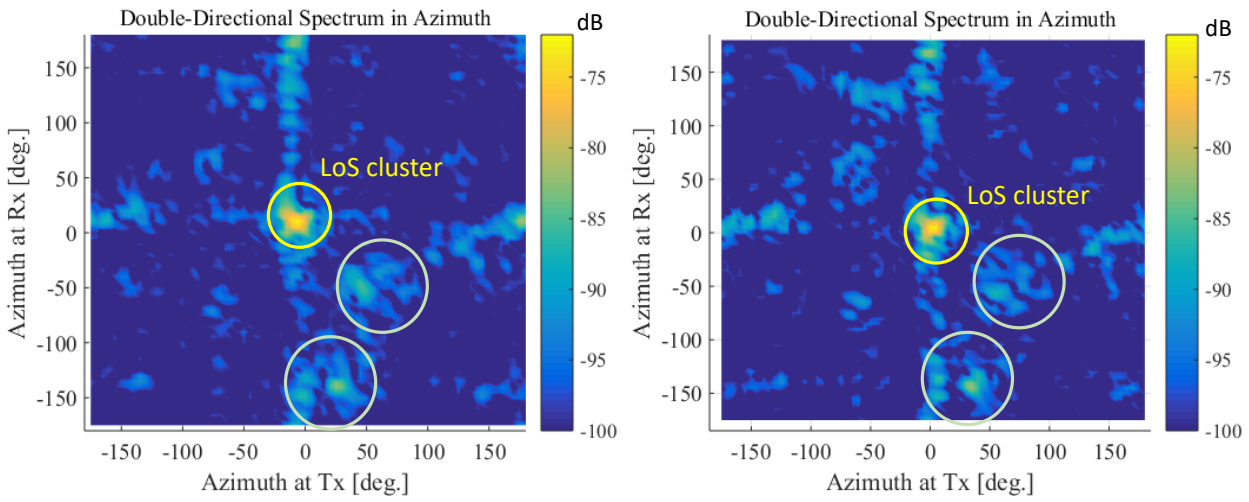

(a)USRP-based system (b)VNA-based system

Figure 7. The double directional power spectrum measurement result (a)USRP-based system, (b)VNA-based system

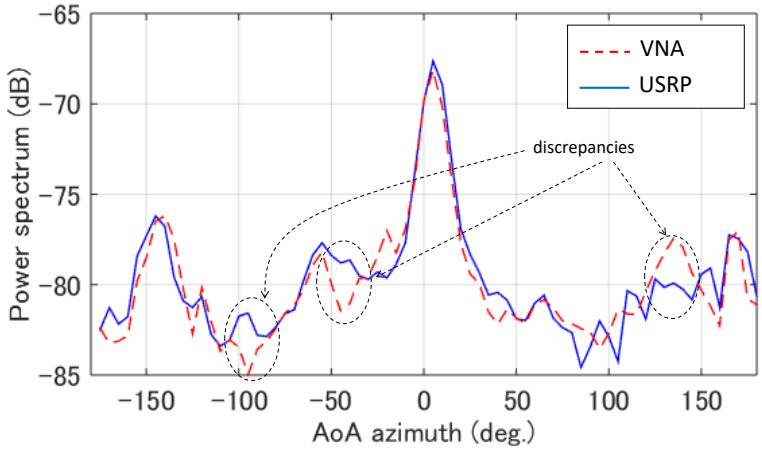

(a) Angle of arrival-side power spectrum

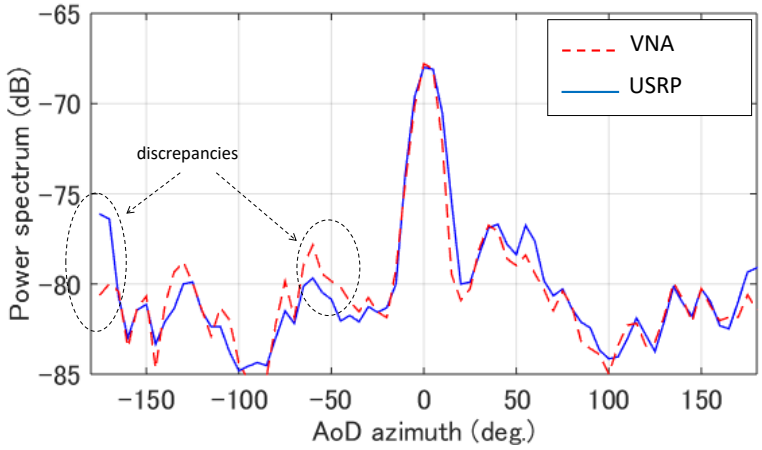

(b) Angle of departure-side power spectrum

Figure 8. The power spectrum comparison (a) Angle of arrival, (b) Angle of departure

The AoD azimuth and the AoA azimuth power spectrum of both the USRP-based system and the VNA-based system are shown in Figure 8 (a) and (b). Although there were some discrepancies which are marked in the figure, differences of power spectra were less than 4 dB. One of the reasons for the differences is thought that the received power variations due to multipath fading. In conclusion, the power spectra of the USRP-based system quite matched with those of the VNA-based system.

Conclusions

This paper presents the development of directional channel sounder on the USRP/GNU radio platform. We solved the data transmission bottleneck of the current channel sounder architecture by accessing the PC's RAM disk from the USRP platform directly and we clarified that the proposed method suppressed sampling losses of data by the cable connected test. We also implemented the virtual array method for evaluation of directional channel properties. We conducted a T-junction cable connected test and an indoor channel measurement and compared the results with the VNA-based measurement system. The result showed that the measurement signal was sampled at correct timings without any sampling losses in our channel sounder. And the error of angular power spectrum of our system was less than 4 dB compared with the VNA based system. The result showed a possibility that the developed channel sounder can be alternatively utilized instead of dedicated measurement instruments. It is expected to be utilized for various kinds of propagation channel measurements.

References

[1] 3GPP, *Requirements for Further Advancements for Evolved Universal Terrestrial Radio Access (E-UTRA) (LTE-advanced)*, 3GPP TR36.913 (V8.0.0) (2008-06), Valbonne, France, 2008.

[2] The Institute of Electrical and Electronics Engineers (IEEE), *IEEE Standard for Information Technology-Telecommunications and Information Exchange between Systems-Local and Metropolitan Area Networks-Specific Regulations Part 11: Wireless LAN Medium Access Control (MAC) and Physical Layer (PHY) Specifications, Amendment 5: Enhancements for Higher Throughput (IEEE Std. 802.11n)*, New York, NY, 2009.

[3] The Institute of Electrical and Electronics Engineers (IEEE), *IEEE Standard for Information Technology-Telecommunications and Information Exchange between Systems-Local and Metropolitan Area Networks- Specific Regulations Part 11: Wireless LAN Medium Access Control (MAC) and Physical Layer (PHY) Specifications, Amendment 4: Enhancements for Very High Throughput for Operation in Bands 6 below 6 GHz (IEEE Std. 802.11ac)*, New York, NY, 2013.

[4] A.F. Molisch, *Wireless Communications*, 2nd Edition, Wiley-IEEE Press, 2010.

[5] M. Steinbauer, A.F. Molisch, and E. Bonek, "The double-directional radio channel," *Antennas and Propagation Magazine, The Institute of Electrical and Electronics Engineers (IEEE)*, Vol. 43, No. 4, pp. 51-63, Aug 2001.

[6] M. Kim, J. Takada, and Y. Konishi, "Novel scalable MIMO channel sounding technique and measurement accuracy evaluation with transceiver impairments," *IEEE Transactions on Instrumentation and Measurement*, Vol. 61, No.12, pp. 3185-3197, 2012.

[7] M. Kim, K. Umeki, K. Wangchuk, J. Takada and S. Sasaki, "Polarimetric Mm-wave

channel measurement and characterization in a small office," *In: The IEEE Proceedings of the 26th Annual International Symposium on Personal, Indoor, and Mobile Radio Communications (PIMRC)*, pp. 764-768, 2015.
[8] 3GPP, *Study on Channel Model for Frequency Spectrum above 6 GHz (Release 14)*, 3GPP TR 38. 900, v14. 0. 0, Valbonne, France, 2016.
[9] ITU-R, *Guidelines for Evaluation of Radio Interface Technologies for IMT-Advanced*, Report ITU-R M.2135, 2009. [Online]. Available: http://www.itu.int/pub/R-REP-M.2135-2008/en
[10] C. Dias, N. Tervo, A. Roivainen, V. Hovinen, M.T. Sonkki, G. Fraidenraich, and M. Latva-aho, "Spatial radio channel sounding for static environment at 10 GHz," In: EurAAP, *2016 10th European Conference on Antennas and Propagation (EuCAP)*, the European Association on Antennas and Propagation (EuCAP), pp. 1-5, 2016.
[11] H. Boeglen, A. Traore, M.M. Peinado, R. Lefort, and R. Vauzelle, "An SDR based channel sounding technique for embedded systems," In: EurAAP, *2017 11th European Conference on Antennas and Propagation (EUCAP)*, pp. 3286-3290, 2017.
[12] N. Costa, and S. Haykin, "A novel wideband MIMO channel model and McMaster's wideband MIMO SDR," In: *2006 Fortieth Asilomar Conference on Signals, Systems and Computers*, IEEE, pp. 956-960, 2006.
[13] A. Merwaday, N. Rupasinghe, I. Guvenc, W. Saad and M. Yuksel, "USRP-based indoor channel sounding for D2D and multi-hop communications," In: *2014 IEEE 15th Annual IEEE Wireless and Microwave Technology*, IEEE, pp. 1-6, 2014.
[14] D. Mass, M.H. Firooz, J. Zhang, N. Patwari, and K.Kasera, "Channel sounding for the masses: Low complexity GNU 802.11b channel impulse response estimation," IEEE Transactions on Wireless Communications, vol. 11, no.1, pp.1-8, Jan. 2012.
[15] M. Tianyang, M. Kim, and J. Takada, "Development of channel sounder using GNU radio/USRP: Timing synchronization and phase alignment," In: *IEICE Technical Report, SR2014-131*, Vol. 114, No. 491, The Institute of Electronics, Information and Communication Engineers, Tokyo, Japan, pp. 121-126, 2015.
[16] S. Enevoldsen, J. Johnasen, and V. Pucci, "*Analysis and Architectural Mapping of an FFT Algorithm into an Already Existing FPGA Firmware of a Low-cost COTS SDR Peripheral*," Thesis(Master's), Aalborg University, Aalborg, Denmark, 2011.